The Shape of Averaged Drop Size Distributions

HENRI SAUVAGEOT AND JEAN-PIERRE LACAUX

Université Paul Sabatier, Laboratoire d'Aérologie (URA.CNRS 354), Toulouse, France

(Manuscript received 24 August 1993, in final form 15 August 1994)

ABSTRACT

The shape of averaged drop size distributions (DSD) is studied from a large sample of data (892 h) collected at several sites of various latitudes. The results show that neither the hypothesis of an exponential distribution to represent rainfall with a high rain rate (R) nor the concept of equilibrium distribution arising from the various models using the parameterization of Low and List is compatible with the observations. To describe the DSD two regions have to be distinguished: a small-drop region, for diameter D smaller than a threshold D_c, and a large-drop region, for diameter D larger than D_c. For $D < D_c$ the distributions are strongly dependent on R and on z_0, the height of fall of the rain from the base of the melting level. The decrease in the relative number of small drops with increasing R suggests that in this region the depletion of the small drops by the big ones is not totally compensated for by the input of small drops due to the collisional breakup process; there is no stationary state for $D < D_c$. In the big-drop region, for $D > D_c$, the slope of the distributions is almost independent of D. At low values of R (<20 mm h^{-1}) it decreases when R increases, and not much depends on z_0. For increasing values of R beyond about 20 mm h^{-1}, the slope of the distributions tends toward a constant value of about 2.2–2.3 mm^{-1}. This suggests a certain stationarity between the coalescence and collisional breakup processes in intense rainfalls. It also appears that the two regions are not much influenced by each other. The value of D_c increases with R and with z_0. The relation between the radar reflectivity factor (Z) and R obtained from the averaged DSDs are close to those calculated from nonaveraged data and compatible with those proposed in the literature. The differences observed between the coefficients of Z–R relations for various types of rain are essentially due to the differences in small-drop concentration.

1. Introduction

The drop size distribution (DSD) is the main term used to describe and discuss rain physics. The DSD and its moments also are the basis of the definition and computation of most parameters intervening in the problems of microwave propagation within clouds and rain, notably in rainfall estimation by radar. That is the reason why many efforts were made to measure, understand, and model the DSDs (Marshall and Palmer 1948; Joss and Gori 1976, 1978; Feingold and Levin 1986, FL hereafter; Zawadski and de Agostinho Antonio 1988, ZA hereafter; Willis and Tattelman 1989, WT hereafter; McFarquhar and List 1991; among many others).

The DSD characteristics depend on microphysical, dynamic, and kinematic processes that interactively influence the falling rain. Srivastava (1978, 1982) suggests that the two main processes controlling the shape of the DSDs are coalescence and collisional breakup. To establish the budget of the competing effects of these two processes, he developed a simple parameterization of them and applied it to an exponential DSD, that is, a DSD for which the number density distribution is

$$N(D) = N_0 e^{-\lambda D}, \tag{1}$$

where D is the spherical drop diameter and N_0 and λ are parameters.

He shows that the DSD evolves with time toward a stationary (or equilibrium) state when the effect of coalescence (which increases the large-drop number and decreases the small-drop number, causing λ to decrease) just balances the effect of collisional breakup (which is the inverse of the coalescence one). In such stationary conditions λ, the slope of the exponential DSD, remains constant, and N_0 is proportional to the rainfall rate R. Constant slopes for large rain rates were also proposed by List and Gillespie (1976) from a numerical model.

There is some observational evidence in support of a constant value of λ for a high rainfall rate (Blanchard and Spencer 1970). The experimental values mentioned in the literature are $\lambda \approx 2.2$–2.3 mm^{-1} for $R > 25$ mm h^{-1} (Mueller and Sims 1966), $\lambda \approx 2.6$ mm^{-1} for $R > 40$ mm h^{-1} (Sekhon and Srivastava 1971), and $\lambda \approx 2.2$ mm^{-1} for a liquid water content $W > 1.2$ g m^{-3} (i.e., $R > 28$ mm h^{-1}) (Pasqualucci 1982). But there is no unanimity and, for example, WT, using a

Corresponding author address: Dr. Henri Sauvageot, Observatiore Midi-Pyrénées, Université Paul Sabatier, CRA 65300 Lannemezan, France.

new set of DSDs in intense rainfall and reanalyzing Mueller and Sims's data, found that λ continues to decrease when R increases beyond 25–40 mm h^{-1}.

Low and List (1982, LL hereafter) proposed from laboratory experiments a sophisticated parameterization of collisional breakup that was used in many numerical modeling studies on the evolution of DSDs in warm rain shafts (Valdez and Young 1985; List et al. 1987, LDS hereafter; Feingold et al. 1988; Brown 1991; Brown and Whittlesey 1992; among others). These studies lead to the conclusions that the DSDs tend to a universal form; that is,

$$N(D, R) = R\psi(D), \qquad (2)$$

where R is the rainfall rate and ψ a generic shape function independent of R. Srivastava's results appear as a particular case of (2) where $\psi(D)$ is exponential. Because the distributions have three peaks (i.e., absolute or secondary concentration maxima for preferential drop sizes) they are called three-peak equilibrium distributions (or 3PED). The 3PED is independent of the DSD considered at the input of the simulation.

Numerical modeling suggests that the 3PED is reached only after a very high number of collisions, that is, in conditions rarely met in nature. Thus, natural rain would approach the 3PED when its rate is high and when its fall height (i.e., the height of the melting level above the ground) is important.

Many field studies were carried out from the ground or by aircraft in order to determine the DSD characteristics. However, there are relatively few data corresponding to conditions compatible with the observation of DSDs that have reached equilibrium. The instrument that is mostly used throughout the world to observe the DSD at the ground is the disdrometer (i.e., the drop size meter, JWD hereafter) devised by Joss and Waldvogel (1967). The peaks announced by the theoretical solutions deduced from Low and List's parameterization were observed using JWD by many investigators on rains of the midlatitudes (Steiner and Waldvogel 1987) and of the tropical latitudes (LDS; List 1988; Asselin de Beauville et al. 1988; ZA). Sheppard (1990) showed that some irregularities in the transfer function of the electronics used for the diameter classification of the raindrops by the JWD were sufficient to produce maxima at diameters similar to those of the peaks. McFarquhar and List (1992) confirmed this result and concluded that "the multiple peak scenarios previously reported by many authors are entirely instrument related." Thus, even if these various works do not prove indisputably the absence of any peak in the DSDs, it appears that the peaks of the mean DSDs measured with the JWD can be considered minor instrumental irregularities and ignored, which is what will be done in this article.

Concerning the small drops, some authors, as indicated above, suppose, without unquestionably proving it, that the discrepancies between observations and theory, when the rain rate is high, can be explained by a technical deficiency of the JWD. In the past, however, many authors have discussed, from observations made without using the JWD, the departure of the DSDs from exponentiality for the small drops. For example, Fujiwara (1965), Cataneo and Stout (1968), and more recently Jones (1992), using raindrop cameras, have observed such a strong lack of small drops that the distributions are close to a skew–symmetric type. Theoretical models (List and Gillespie 1976; Brazier-Smith et al. 1973) support these observations by suggesting that the depletion of the smallest drops results from their collection by larger ones. Such a departure from exponentiality led some authors to propose the representation of the DSDs in the general case (notably including the tropical DSDs) not by the classical exponential, which is representative of weak to moderate rainfalls in midlatitudes, but by gamma (Ulbrich 1983) or lognormal (FL) three-parameter distributions.

It thus appears that there is currently no general agreement on the shape of the raindrop distributions. The validity of the concept of DSD at equilibrium is not confirmed. The existence in the DSDs of characteristics independent from the rate, that is, an account of the evolution toward a shape reflecting an equilibrium between coalescence and collisional breakup processes, needs to be cleared up. It is the same with the evolution with R of the relative number of the small drops.

The object of this paper is to present the results of a study of the DSD shape according to the rainfall rate from the analysis of a large data sample. The study focuses more particularly on the evolution with R of the DSD slope and the relative number of the small drops. These two characteristics are indeed pertinent to the discussion of an evolution toward an equilibrium between coalescence and collisional breakup. The relations between the DSD moments are also discussed. The sample used contains 53 531 DSDs with a time resolution of 1 min (i.e., more than 892 h) measured at the ground in sites located along a north–south direction, from the midlatitudes up to the equator, on rain associated with stratiform and convective systems. The rain rates cover a large range (up to 170 mm h^{-1}) with heights below melting level up to ~5500 m.

2. Data

a. The sensor

The measurements were made with a JWD. This instrument converts the vertical mechanical moment of the drops into electric pulses. The sampling area measures 50 cm^2. Only drops with a volume larger than a threshold corresponding to a 0.3-mm equivalent spherical diameter are detected. The pulses are converted to 8-bit numbers and sorted according to 25 size classes, all with the same width ΔD = 0.2 mm, covering di-

ameters ranging from 0.3 to 5.3 mm. The appendix presents a set of experimental arguments showing that the small relative number of small drops possibly observed with the JWD is essentially real and that the instrumental cause is marginal. The data were systematically corrected for the error due to dead time of the instrument after the sampling area is hit by the drops (see the appendix). The measurement time span of a DSD is always 1 min.

b. The sample

The data sample used was collected at four sites (Fig. 1 and Table 1).

1) A midlatitude site, Brest in Brittany (48°25′N, 4°25′W; altitude 30 m) during a French–British cooperative campaign called Fronts 87 in the winter of 1987/88. In Brittany, most of the precipitation is associated with the frontal cyclonic systems of the zonal circulation. In winter, these systems are well developed with extended stratiform precipitation at the level of the warm front and a cold front associated with deep convection. The mean annual total rainfall is about 1200 mm. The region is flat.

2) An equatorial site, Abidjan (5°25′N, 4°W; altitude 40 m), on the southern Ivory Coast, on the Guinea Gulf coast, in 1986–87 and 1988. In this area, it is possible to distinguish clearly a long rainy season from March to mid-July, associated with the northward migration of the intertropical convergence zone (ITCZ), and a short rainy season from mid-September to late November, associated with southward migration of the ITCZ. The mean annual total rainfall is about 1800 mm. The region is flat.

Two sites of continental Africa were chosen.

3) Niamey, in southwestern Niger (13°30′N, 2°10′E; altitude 220 m) during the rainy season (which lasts about three months, from early July to late September) in 1988 and 1989. Niamey is situated in the middle of the Sahelian Sudanese strip. The mean annual total rainfall is about 500 mm. The rainy season is associated with the northward move of the ITCZ. The area is very flat. The most significant rain-generating events are organized in squall lines with a very pure structure (Desbois et al. 1988). On this site, there was also a numerized *C*-band radar (Sauvageot and Despaux 1989).

4) Boyélé, in the northern Congo (2°50′N, 18°04′E; altitude 330 m) in 1988 and 1989. Boyélé is located in the upper basin of the Oubangui River in a region locally flat. The mean annual pluviometry is about 1000 mm. The rainy season lasts from early March to late November. The measurement station was situated in the Pygmy area, in a vast clearing surrounded by the primary equatorial forest. The main precipitating systems are also organized in squall lines there.

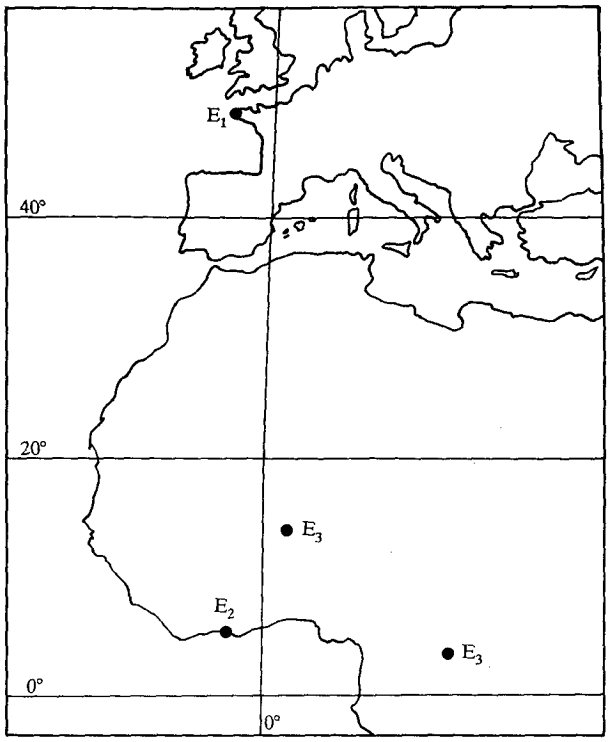

FIG. 1. Location of the data collection sites (see Table 1).

The data of the two continental African sites were gathered in only one sample since they correspond to the same meteorological entity and since the DSD characteristics are essentially identical there.

c. Averaging the DSD

The characteristics of the DSDs observed depend on the integration conditions in time and space of the measurement (see Joss and Gori 1976, 1978; Smith et al. 1993). The "instantaneous" DSDs, that is, those measured during a short interval, generally have a strong variability, due, for example, to kinematic effects on the drops trajectory (vertical shear of the horizontal wind, updraft, cellularity of the rain, etc.).

The sampling resolution time of 1 min used to obtain the DSDs is an interesting compromise since, at the translation velocities of the rain-bearing systems, it corresponds to a displacement comparable to the mean size of the radar pulse volume; it can thus be used for the analysis of the variations of some integral parameters useful to discuss the radar measurements (notably R and the radar reflectivity factor Z).

To obtain significant estimations of the parameters describing the DSDs that can be compared with the theoretical results, it is necessary to average the instantaneous DSDs in order to eliminate the randomly varying components and to obtain stable distributions.

TABLE 1. Data sample designation. Here R is rain rate and z_0 is the mean altitude of melting level during the rainy season.

Location	France	Ivory Coast	Niger–Congo	
Designation of the sample	E_1 Midlatitude	E_2 Equatorial Africa	E_3 Continental Africa	
Number of 1-min DSD in the sample	9021	27 126	17 384	53 531
R_{max} (mm h^{-1})	54	150	170	
z_0 (km asl)	Winter: 1.0 Summer: 2.4	4.1	Niger: 5.2 Congo: 4.2	

3. Averaged distributions

The instantaneous DSDs of each sample were gathered in eight classes for the tropical rains and seven classes for the midlatitude rains as indicated in Table 2. Figure 2 shows the average distributions for the various rain-rate classes for the three samples E_1 to E_3. For increasing values of the parameter R, for diameters larger than the mode, the slope of the distributions is first seen to decrease then tends to become constant. When R increases, the relative number of the small drops decreases for the three samples. The weakness of the small-drop number increases from E_1 to E_3. For the two larger rain rates of E_3 ($R > 40$ mm h^{-1}) the first three classes are empty; that is, there are no drops with $D < 0.8$ mm.

To enable the comparison of these various distributions, the fitting parameters to analytical distributions were calculated. The fitting to an exponential distribution will be considered in section 4. To quantify the general shape of the distributions, notably the relative quantity of small drops, the lognormal distribution was used. To represent the DSDs, which show a lack of small drops compared to the exponential distribution, various types of three-parameter distributions can be used; their compared advantages were defended and illustrated, notably by Ulbrich (1983) for the modified gamma distribution, and by FL for the lognormal distribution. The modified gamma distribution causes a relatively serious inconvenience, which is that the dimension of one of the parameters (N_0) depends on another one (μ), which introduces a functional dependence between these two parameters (FL; Chandrasekar and Bringi 1987).

For the present study, three three-parameter distributions were compared: modified gamma, complete gamma, and lognormal. All give acceptable results. The lognormal distribution was chosen because the parameters have a simple geometrical interpretation and because the moment generating function can be written very simply in the form of a multiplication of three terms, each being a function of only one of the three parameters (this property will be used in section 5).

The lognormal distribution has the following expression:

$$N(D) = \frac{N_T}{(2\pi)^{0.5}(\mathrm{Ln}\sigma)D} \times \exp[-\mathrm{Ln}^2(D/Dg)/(2\,\mathrm{Ln}^2\sigma)], \quad (3)$$

where N_T is the total number of drops, Dg is the mean geometrical diameter, and σ is the standard geometrical deviation of D; namely,

$$N_T = \int_0^\infty N(D)dD, \quad (4)$$

$$\mathrm{Ln}Dg = \overline{\mathrm{Ln}D}, \quad (5)$$

$$\mathrm{Ln}^2\sigma = \overline{(\mathrm{Ln}D - \mathrm{Ln}Dg)^2}. \quad (6)$$

In Fig. 3, the variation of the three parameters according to R was represented for each of the three samples.

The value of N_T increases as a function of R with a derivative decreasing, that is, as a power function of R with the power n such as $0 < n < 1$. Here N_T, for a given value of R, is the highest for E_1 (many small drops) and the lowest for E_3 (few small drops). For E_1 however, beyond $R = 10$ mm h^{-1}, N_T rapidly decreases to finally follow the curve of E_2. For Dg, an increase proportional to R^n with $0 < n < 1$ can also be observed, but Dg is the highest for E_3 and the lowest for E_1.

Figure 3 shows that σ does not vary much with R, so that $\sigma(R)$ can be represented relatively correctly by a linear function (Table 3). For E_2, the $\sigma(R)$ relation is similar to that obtained by FL in Israel (see Table 3); that is, σ is nearly constant. For E_1 and E_3, the amplitude of the variation of σ, when R varies, is about 10 times stronger than for E_2. This fact is important because the value of the exponential in the expression of the moments of $N(D)$ is very sensitive to that of σ.

The various functions fitted for the three parameters of the three samples are indicated in Table 3. The functions computed by FL were also indicated in Table 3 for comparison. In Table 3, the relations between these parameters and R, calculated on our samples, can be seen to be very tight [correlation coefficient close to 1, except for $\sigma(R)$ of E_2 because σ is nearly independent of R].

Each parameter of the lognormal distribution can thus be expressed by a function of R alone. However, these coefficients are different for the three samples and

TABLE 2. Parameters of the averaged DSDs for the three samples of Table 1. Here R, W, Z, and D_0 are the rain rate, the liquid water content, the radar reflectivity factor, and the mean volume diameter, respectively. Also, N_0 and λ are the exponential distribution paramaters (1) obtained by regression on the classes whose size is larger than the mode of the distribution; ρ is the correlation coefficient of the fitting; and N_T, D_g, and σ are the parameters of the lognormal distribution (3).

Sample name		Class of rain rate (mm h^{-1})	Number of DSD of 1 min	R (mm h^{-1})	W (g m^{-3})	Z (dBZ)	D_0 (mm)	Exponential N_0 (m^{-3})	Exponential λ (mm^{-1})	Exponential ρ	Lognormal N_T (m^{-3})	Lognormal D_g (mm)	Lognormal σ
E_1	R_1	$R < 2$	8065	0.4	0.024	18.0	0.92	2474	4.04	0.99	184	0.49	1.52
	R_2	$2 < R < 4$	646	2.7	0.037	29.0	1.19	4694	3.12	0.99	542	0.58	1.59
	R_3	$4 < R < 6$	230	4.9	0.075	33.0	1.38	4793	2.80	0.99	604	0.64	1.61
	R_4	$6 < R < 8$	85	6.9	0.34	34.9	1.47	5560	2.74	0.99	671	0.67	1.66
	R_5	$8 < R < 10$	55	9.0	0.42	36.7	1.61	5017	2.53	0.99	714	0.69	1.66
	R_6	$10 < R < 15$	60	12.0	0.55	38.6	1.75	6854	2.44	0.99	584	0.85	1.68
	R_7	$15 < R$	60	23.7	0.91	43.8	2.08	8234	2.07	0.99	442	1.12	1.70
E_2	R_1	$R < 2$	18 340	0.4	0.02	18.7	1.17	1373	3.28	0.99	38	0.93	1.42
	R_2	$2 < R < 4$	2967	2.9	0.14	29.6	1.30	7384	3.29	0.99	152	1.06	1.36
	R_3	$4 < R < 6$	1342	4.9	0.24	32.5	1.41	9325	3.15	0.99	221	1.17	1.34
	R_4	$6 < R < 10$	1282	7.7	0.36	35.0	1.51	6583	2.67	0.99	268	1.24	1.33
	R_5	$10 < R < 20$	1366	13.9	0.80	40.1	1.76	9741	2.53	0.99	345	1.34	1.32
	R_6	$20 < R < 40$	1098	28.4	1.06	42.9	1.97	13 933	2.33	0.99	461	1.50	1.34
	R_7	$40 < R < 60$	453	47.6	1.81	47.2	2.17	25 878	2.23	0.99	509	1.68	1.33
	R_8	$60 < R$	280	76.9	2.96	50.3	2.34	36 772	2.15	0.99	575	1.83	1.34
E_3	R_1	$R < 2$	9388	0.6	0.04	24.9	1.18	1662	3.31	0.99	60	0.81	1.49
	R_2	$2 < R < 4$	1806	3.0	0.14	33.4	1.62	3356	2.85	0.98	145	1.01	1.43
	R_3	$4 < R < 6$	1440	4.6	0.23	35.5	1.65	3619	2.57	0.99	172	1.13	1.41
	R_4	$6 < R < 10$	1362	7.8	0.36	38.2	1.83	5809	2.51	0.99	202	1.30	1.37
	R_5	$10 < R < 20$	1134	14.8	0.60	43.1	2.02	11 612	2.50	0.99	231	1.48	1.36
	R_6	$20 < R < 40$	1066	27.0	1.07	45.7	2.24	17 652	2.25	0.99	246	1.83	1.30
	R_7	$40 < R < 60$	936	48.0	1.80	48.9	2.39	31 261	2.20	0.99	316	2.08	1.27
	R_8	$60 < R$	252	73.4	2.70	50.9	2.46	65 343	2.29	0.99	415	2.18	1.25

different from those of FL. For each sample, a tight relation between N_T and Dg can be written, but the coefficients of these relations are different from one sample to another.

4. Discussion

Globally, what has been said clearly shows that neither the hypothesis of an exponential distribution to represent rainfalls with a strong rain rate nor the concept of equilibrium distribution resulting from the various models using the parameterization of LL, notably the expression of this concept by an equation of the form of (2), is compatible with the observation.

Figure 4 shows the distribution R_7 (47.7 mm h^{-1}) from the E_2 sample, the distribution R_7 (48 mm h^{-1}) from the E_3 sample, the theoretical distribution given by the LDS model for $R = 48$ mm h^{-1}, and the slope of the exponential distribution for $\lambda = 2.25$ mm^{-1}. It can be seen that the curves are in agreement between about 2 and 2.7 mm but that the slope of the theoretical distribution is markedly steeper than the experimental ones for $D > 3$ mm and that the high concentration of small drops prescribed by the theory is not observed in the data.

Figure 5 shows the variation with R, for the E_1 to E_3 samples, of the n_s/n_L ratio defined as

$$\frac{n_s}{n_L} = \int_{D_{\min}}^{D_1} N(D)dD \Big/ \int_{D_1}^{D_{\max}} N(D)dD, \qquad (7)$$

where D_1 is a diameter arbitrarily taken at 1.7 mm. If $N(D)$ is represented by (2), the n_s/n_L ratio is constant whatever the value of R. Figure 5 shows that this ratio is not constant at all but strongly dependent on R. It decreases when R increases, and for a same value of R, it is higher at the midlatitudes than at the tropical latitudes.

Figure 2 and Table 2 show that, for the rain rate classes such as $R > 20$ mm h^{-1}, the slope of the distribution is constant or does not vary much on the side of the large diameters. To make the following discussion easier, two domains will be schematically distinguished in the DSDs: that of the small drops such as $D < Dc$, and that of the large drops such as $D > Dc$. Here Dc is the threshold, variable according to R, above which the slope of the DSDs is constant.

To quantify the value of the slope and the range of independence from R, the parameters λ and N_0 of the fitting of the DSDs to an exponential distribution were calculated. The exponential distribution is given by (1) with $N(D)$ and N_0 (mm^{-1} m^{-3}) and λ (mm^{-1}). For this fitting, only the points corresponding to the diameters equal to or larger than D_c were considered. The results are given in Table 2. It can be noted that the fitting is very tight (correlation coefficients are higher than 0.98). Figure 6a shows the value of the exponential fit

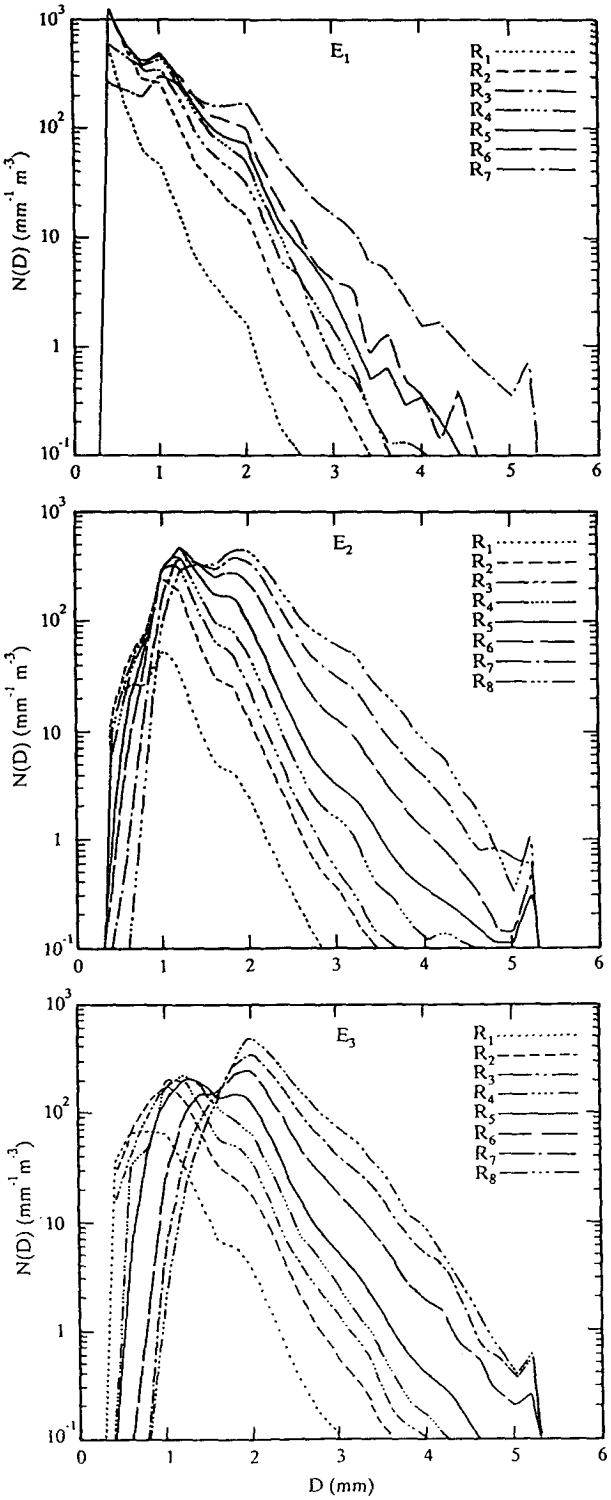

FIG. 2. Averaged DSDs for the three samples E_1, E_2, and E_3, for the rain-rate classes of Table 2.

slope parameter λ versus R. The equation of the curve fitted to the $\lambda - R$ points for the tropical samples (i.e., E_2 and E_3) is (Fig. 6a)

$$\lambda = 3.2R^{-0.09}, \quad (8)$$

where λ (mm^{-1}) and R (mm h^{-1}). The correlation coefficient $\rho = 0.92$.

For the E_1 midlatitude sample, we have

$$\lambda = 3.6R^{-0.16}, \quad (9)$$

with $\rho = 0.99$.

For a comparison, the $\lambda(R)$ curve of the Marshall–Palmer (1948) distribution was drawn; the equation is

$$\lambda = 4.1R^{-0.21}. \quad (10)$$

The N_0/λ ratio, equal to the zero moment of (1), that is, to the total number of drops N_T of the distribution, can be found in Fig. 6b. Here N_0/λ is seen to increase with R. The equation of the curve is

$$\text{for } E_2 + E_3, \quad N_T = 670R^{0.74}, \quad (11)$$

with $\rho = 0.97$.

$$\text{For } E_1, \quad N_T = 890R^{0.44}, \quad (12)$$

with $\rho = 0.99$.

For low R values λ decreases sharply when R increases, but λ is seen to be roughly constant, around 2.2–2.3 mm^{-1} for $R > 20$ mm h^{-1}.

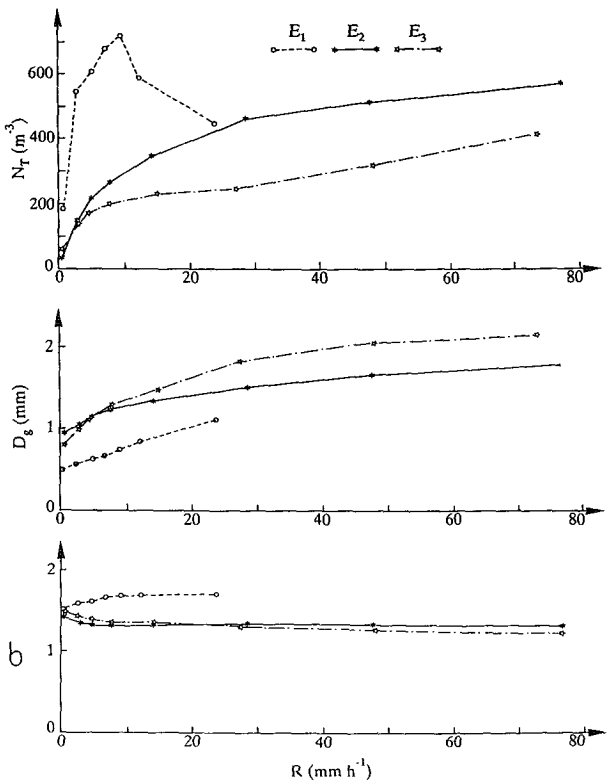

FIG. 3. Variation of the lognormal distribution parameters N_T, D_g, and σ for E_1, E_2, and E_3 as a function of R. The data used to plot the curves are given in Table 2.

TABLE 3. Analytical functions fitted between various parameters and the rain rate R. Here N_T, D_g, and σ are the parameters of the lognormal distribution (3); H is the exponential of (15); Σ, W, and Z are optical extinction, liquid water content, and radar reflectivity factor, respectively. Also, ρ is the correlation coefficient of the fitting. The Z_0–R relations were obtained by direct regression of the raw data at the 1-min time resolutions. The results of FL are also given. Values for N_T, D_g, Z, R, Σ, and W are in m^{-3}, mm, $mm^6\ m^{-3}$, mm h^{-1}, km^{-1}, and g m^{-3}.

E_1 Midlatitude	E_2 Equatorial Africa	E_3 Continential Africa	FL
$N_T = 323R^{0.26}$	$N_T = 80R^{0.51}$	$N_T = 86R^{0.36}$	$N_T = 172R^{0.22}$
$\rho = 0.74$	$\rho = 0.98$	$\rho = 0.98$	
$D_g = 0.52R^{0.18}$	$D_g = 0.97R^{0.13}$	$D_g = 0.84R^{0.23}$	$D_g = 0.72R^{0.23}$
$\rho = 0.90$	$\rho = 0.97$	$\rho = 0.99$	
$\sigma = 1.57 + 7 \times 10^{-3}R$	$\sigma = 1.36 - 4 \times 10^{-4}R$	$\sigma = 1.42 - 3 \times 10^{-3}R$	$\sigma = 1.43 - 3 \times 10^{-4}R$
$\rho = 0.83$	$\rho = 0.35$	$\rho = 0.89$	
$H_2 = 1.47R^{0.064}$	$H_2 = 1.23R^{-0.014}$	$H_2 = 1.35R^{-0.047}$	
$\rho = 0.96$	$\rho = 0.78$	$\rho = 0.98$	
$H_3 = 2.37R^{0.15}$	$H_3 = 1.60R^{-0.031}$	$H_3 = 1.97R^{-0.11}$	
$\rho = 0.96$	$\rho = 0.78$	$\rho = 0.98$	
$H_{3.67} = 3.64R^{0.22}$	$H_{3.67} = 2.01R^{-0.046}$	$H_{3.67} = 2.76R^{-0.16}$	
$\rho = 0.96$	$\rho = 0.78$	$\rho = 0.98$	
$H_6 = 34R^{0.49}$	$H_6 = 6R^{-0.12}$	$H_6 = 13R^{-0.38}$	
$\rho = 0.96$	$\rho = 0.78$	$\rho = 0.98$	
$\Sigma = 0.20R^{0.68}$	$\Sigma = 0.15R^{0.76}$	$\Sigma = 0.13R^{0.77}$	
$W = 0.056R^{0.95}$	$W = 0.061R^{0.87}$	$W = 0.053R^{0.94}$	
$Z = 216R^{1.83}$	$Z = 400R^{1.17}$	$Z = 392R^{1.36}$	$Z = 200R^{1.6}$ (with $\sigma = 1.41$)
$Z_0 = 228R^{1.62}$	$Z_0 = 369R^{1.28}$	$Z_0 = 364R^{1.36}$	
$\rho = 0.98$	$\rho = 0.98$	$\rho = 0.98$	

A constant slope for the values of R higher than about 20 mm h^{-1} was observed by Mueller and Sims (1966), Sekhon and Srivastava (1971), and Pasqualucci (1982) but denied by WT. Willis and Tattelman work on DSDs of high rain rate. They use data collected by aircraft at two altitude levels, 3000 and 450 m, with optical sensors, and reanalyze the data at the ground of Mueller and Sims (1966), which also corresponds to high rainfall rates. They find that λ goes on decreasing when R increases. Figure 7 gathers on the same plot the four curves presented separately in WT's Fig. 3; those are four average DSDs observed at an altitude of 450 m for four rain-rate classes = 25–62.5 mm h^{-1} (a), 62.5–125 mm h^{-1} (b), 125–225 mm h^{-1} (c), and >225 mm h^{-1} (d). Figure 7 shows that, beyond a diameter Dc ranging from 2 mm (panel a) to 3.5 mm (panel d), the slope is constant with a value of λ of about 2.2–2.3 mm h^{-1}. For $D < Dc$, the small-drop number varies little according to R, which shows very well, compared with the exponential, a lack of small drops, which becomes worse when R increases. As a result, if the DSDs of Fig. 7 are fitted to an exponential distribution for $D > 1$ mm, as WT do it, a value of λ that goes on decreasing when R increases beyond 20 mm h^{-1} is obtained. The WT data are thus totally compatible and in agreement with one of the conclusions of the present work—namely, that the constance of the DSD slope for high values of R is verified only when D is above a certain threshold Dc, which depends on R.

The examination of the average DSDs, established according to the Mueller and Sims data presented by WT, also shows that the small-drop proportion for comparable rates is less important for the tropical observation sites than for those of the midlatitude.

The comparison of the average DSDs observed by WT for the same rate classes at the altitudes of 3000 and 450 m (Figs. 2 and 3 in WT) shows that, in all the cases presented, the proportion of the small drops in the DSDs is less important in the DSDs observed at low level, while the slope for $D > Dc$ is not sensibly modified.

Figures 8a and 8b concerns the slope of the DSDs for $R < 20$ mm h^{-1}, that is, in the nonstationary field. It shows, as an example, the DSDs corresponding to the three samples E_1 to E_3 superimposed on a same plot, for values of R ranging from 2.7 to 3 mm h^{-1} (panel a) and from 12 to 14.8 mm h^{-1} (panel b). The slope of the DSDs for $D > Dc$ in each of the two cases is found to be almost identical for the three samples. The curves and conclusions are identical for the other DSDs (for $R < 20$ mm h^{-1}). The three samples correspond to very different rainfall heights; the fall height of the rain thus does not strongly influence the slope of the distributions for $D > Dc$.

The experiment suggests the following.

1) In all the fields of R, the proportion of small drops and the shape of the DSDs for $D < Dc$ depend not only on R but also on the fall height of the rain, that is, the height of the precipitation melting level (z_0) (see Table 1). This shows that the depletion of the small drops by coalescence is not totally compensated for by the production by the breakup, and thus that

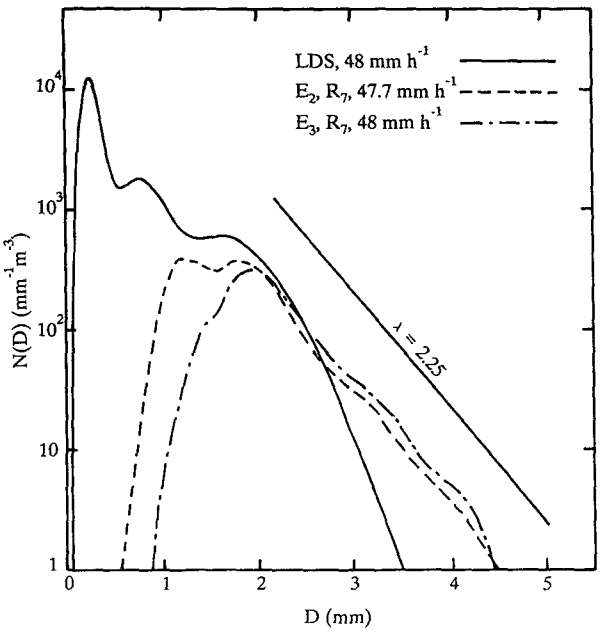

FIG. 4. Averaged DSDs for R_7 of E_2 and E_3 and theoretical 3PED given by the LDS model for the same rain rate (48 mm h^{-1}). The straight line shows the slope of the exponential distribution for $\lambda = 2.25$ mm^{-1}.

there is no stationary shape in this area of the DSDs. The value of Dc, that is, the width of the domain of D influenced by the depletion, which is not compensated for, also depends on R and on the rainfall height.

2) At the low values of R (i.e., $R < 20$ mm h^{-1}), the slope for $D > Dc$ essentially depends on R and not much on the site (i.e., of z_0).

3) For $R > 20$ mm h^{-1} (i.e., for a water content $M > 1$ gm^{-3}) the slope of the DSD for $D > Dc$ tends to be constant. This can be understood as showing some equilibrium between the coalescence and collisional breakup processes in the falling rain. However, the experiment suggests that the processes responsible for the evolution of the DSDs, for the $D > Dc$ domain, and whatever the value of R, seem little influenced by those of the $D < Dc$ domain. In the same way, the stationary slope seems to be the same everywhere (around 2.25 mm^{-1}), which tends to show that it is not necessary, to reach the stationary state, to have a fall height as dramatic as LDS and followers contend.

5. Relation between the moments of $N(D)$

The concept of equilibrium distribution described by (2) implies, as indicated by Hodson (1986), List (1988), and ZA, that the radar reflectivity factor is a linear function of the rain rate. Indeed, by definition,

$$Z = \int_{D_{\min}}^{D_{\max}} D^6 N(D, R) dD;$$

that is, with (2),

$$Z = R \int_{D_{\min}}^{D_{\max}} D^6 \psi(D) dD = RC, \qquad (13)$$

where C is a constant. List (1988) finds for C a value of 742 mm^6 m^{-3} $(mm\ h^{-1})^{-1}$ with Z (mm^6 m^{-3}) and R (mm h^{-1}), which he suggests is a universal constant for the steady tropical rains. Such a linearity is generally not observed in nature.

The object of this section is to examine whether the DSDs presented in section 3 and in Table 2, and parameterized as indicated in Table 2, lead to Z–R relationships compatible with observation.

The generating function of the moments of $N(D)$, that is,

$$m_n = \int_0^{\infty} D^n N(D) dD, \qquad (14)$$

can be written for lognormal $N(D)$ [Eq. (3)]:

$$m_n = N_T D_g^n \exp\left[\left(\frac{n^2}{2}\right) \mathrm{Ln}^2\sigma\right]. \qquad (15)$$

We saw in section 3 and Table 3 that N_T and D_g can be expressed by power functions or R. The relationships between the exponential in (15) and R were also sought. Let H_n be this exponential; that is,

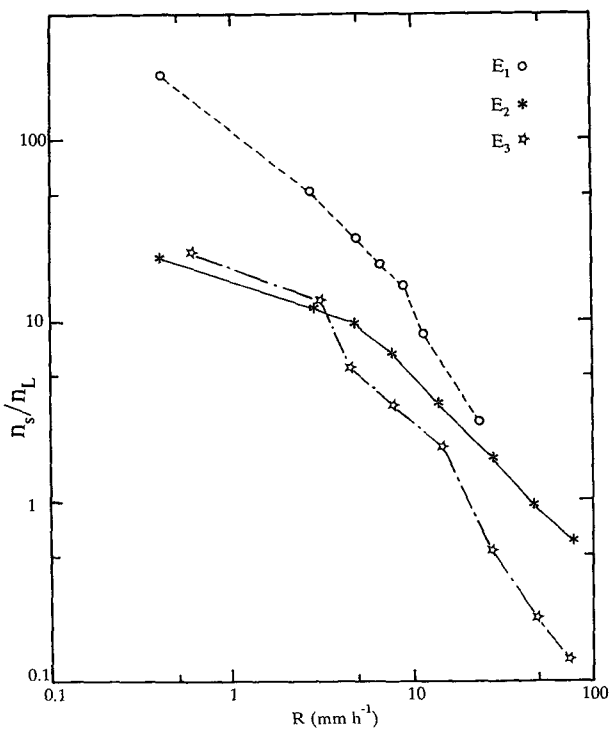

FIG. 5. Plot of the ratio n_s/n_L as a function of R for the samples E_1 to E_3. Here n_s and n_L are the number of drops with diameters <1.7 mm and >1.7 mm, respectively.

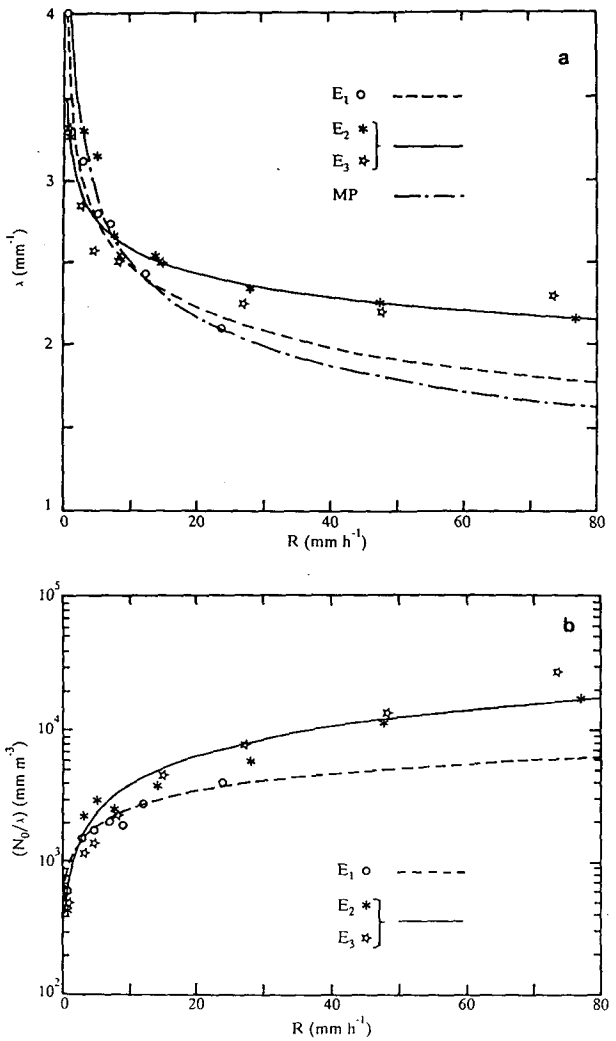

FIG. 6. (a) Variation of λ [Eq. (1)] versus R. The solid line is the fitted curve for $E_2 + E_3$ [Eq. (8)], the dashed line is for E_1 [Eq. (9)], and the dashed–dot line is the Marshall–Palmer relation [Eq. (10)]. (b) Variation of N_0/λ versus R with the same symbols as in (a). The solid line is for Eq. (11); the dashed line is for Eq. (12).

$$H_n = \exp\left[\left(\frac{n^2}{2}\right)\mathrm{Ln}^2\sigma\right]. \tag{16}$$

The relations between H_n and R are found to be well represented by power functions. The relations obtained for $n = 2$, 3, 3.67, and 6, that is, for values of n corresponding to the optical extinction Σ, to the liquid water content W, to the rainfall rate R, and to the radar reflectivity factor Z, respectively, are indicated in Table 3. In Table 3, the correlation coefficients are found to be generally high ($\rho > 0.98$). So m_n, which is the product of three power functions of R, is also a power function of R; namely,

$$m_n = N_T(R)D_g^n(R)H_n(R) = a_nR^{bn}, \tag{17}$$

where a_n and b_n are coefficients.

The integral rainfall parameters of interest P_n, such as the radar reflectivity factor or the rainfall rate, are proportional to m_n; that is,

$$P_n = C_nm_n, \tag{18}$$

where C_n is a coefficient. Using (17) in (18), we have

$$P_n = C_na_nR^{bn}. \tag{19}$$

If the terminal fall velocity of the drops in still air is represented by the power function

$$V(D) = 3.78D^{0.67}, \tag{20}$$

with D in millimeters and $V(D)$ in meters per second (Atlas and Ulbrich 1977), it is easy to see that the analytical expression of the rainfall rate R is proportional to $m_{3.67}$. We thus have $P_{3.67} = R$, which if we take (19) into account, implies that for $n = 3.67$, we must have

$$C_na_n \approx b_n \approx 1. \tag{21}$$

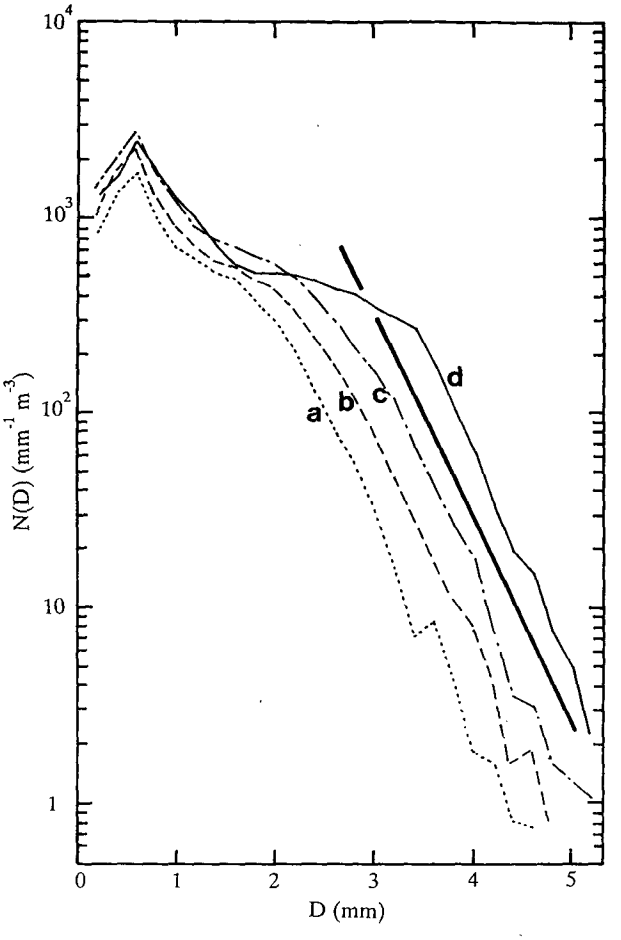

FIG. 7. Mean DSDs from observation at 450-m altitude for rain rates (a) 25–62.5 mm h^{-1}, (b) 62.5–125 mm h^{-1}, (c) 125–225 mm h^{-1}, and (d) >225 mm h^{-1}. The heavy line shows the slope of the exponential distribution for $\lambda = 2.3$ mm^{-1} (adapted from Willis and Tattelman 1989).

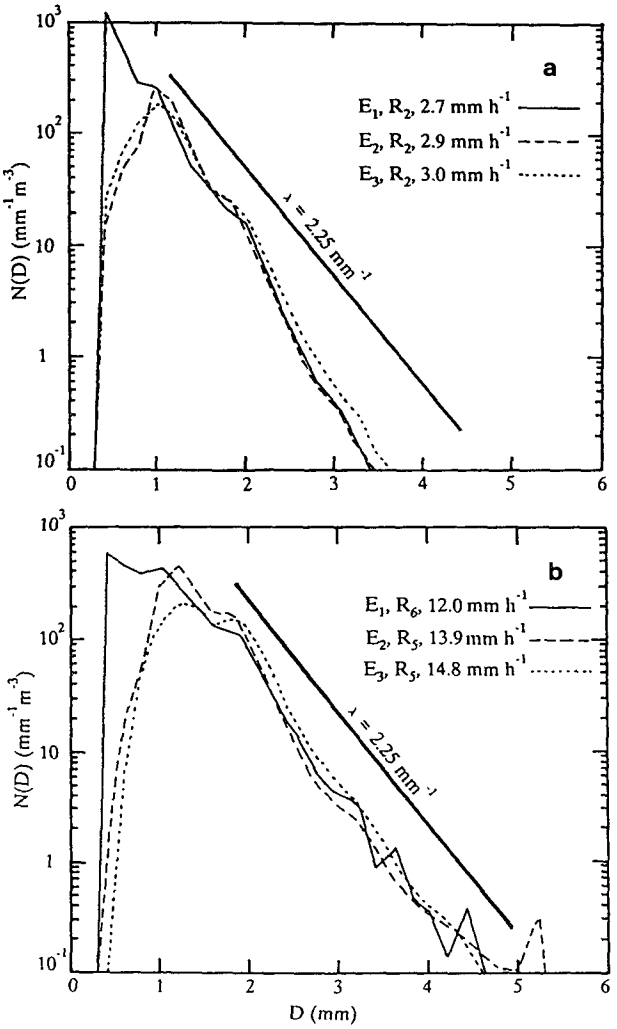

FIG. 8. Averaged DSD for the three samples (E_1 to E_3) and for the same rain rates. (a) For R ranging from 2.7 to 3 mm h^{-1} and (b) for R ranging from 12 to 14.8 mm h^{-1}. The heavy line shows the slope of the exponential distribution for $\lambda = 2.25$ mm^{-1}.

The constraint expressed by (21) can be used to check the consistency of the relations fitted from the data given in Table 3. In Table 4 are indicated the results obtained for $C_n a_n$ and b_n for samples E_1 to E_3 from the coefficients of the relations of Table 3, as well as those deduced from the relations given by FL. The computed values can thus be found to be close to 1; the results of the verification are thus positive.

The functions of Table 3 were used to calculate the $P_n(R)$ relations for the integral parameters of interests, for the samples E_1 to E_3 and for FL's data. We also indicated the results obtained for Z–R by direct regression of the data at the 1-min time step. There is a good agreement for Z–R between the relation deduced from Table 3 and nonaveraged data. Moreover, the coefficients are compatible with the universal observation that for the mostly convective rains of the tropical latitudes, the coefficients a and b of $Z = aR^b$ are higher and lower, respectively, than for the rains, including an important stratiform component, of the midlatitudes. The FL data lead to coefficients that are exactly those of the Marshall–Palmer relation (1948).

Taking into account the discussion above and notably the fact that the DSD slope for $D > D_C$ essentially depends on R, it appears that the differences observed between the coefficients of the relations Z–R are essentially due to the differences in the small-drop concentrations.

6. Conclusions

This paper presented a study of the DSD shape according to the rainfall rate from the analysis of a large sample of data collected at several sites of various latitudes. It is shown (in the appendix) that the JWD, used for the observations, correctly measures the rainfall rates and that the lack of small drops compared with the exponential distribution is real and not instrumental.

The results lead to the following conclusions. The representation of the raindrop spectra by exponential distributions, as well as the concept of equilibrium distribution of LDS and followers, is incompatible with the observations. The incompatibilities concern the small-drop distribution as well as the large-drop one.

To describe the characteristics of the raindrop spectra, we suggested that two regions in the DSD be distinguished: a small-drop region where $D < Dc$ and a large-drop region where $D > Dc$. Here Dc is a threshold variable with R. It can be defined as the diameter above which $dN(D)/dD$ = constant.

The DSDs for $D < Dc$ are strongly dependent on R and on the rainfall height (z_0). This suggests that in this region the depletion of the small drops by the big ones is not totally compensated for by the input of small drops due to the collisional breakup process. So there is no stationary state of the DSDs for $D < Dc$. The value of the $D = Dc$ threshold increases with R for the same site and increases when the latitude decreases (i.e., when z_0 is important). In the large-drop region, the slope λ (for $D > Dc$) is almost independent of D. At low values of R (<20 mm h^{-1}) it decreases when R increases and is not much dependent on the site (i.e., on z_0). For increasing values of R beyond about 20 mm h^{-1}, the slope λ tends toward an almost constant

TABLE 4. Checking of the consistency of the relations given in Table 3 [i.e., Eq. (21) with $n = 3.67$]. The values calculated for FL are also given.

Sample	$C_n a_n$	b_n
E_1	0.76	1.14
E_2	1.07	0.94
E_3	0.89	1.04
FL	0.87	1.06

value, independent of R and of the site, of about 2.2–2.3 mm^{-1}. This evolution suggests a certain stationarity between the coalescence and collisional breakup processes in intense rainfalls. It also seems that the shape of the DSDs for $D > Dc$ is not much influenced by that of the region corresponding to $D < Dc$.

The averaged drop spectra were represented by log-normal distribution (as suggested by FL). In this case, the moments of the DSDs are found to be the product of three power functions of R and thus themselves power functions of R. They can thus be used to compute the relations between Z and R. The Z–R relations obtained from the averaged DSDs are close to those calculated from nonaveraged data and compatible with those proposed in the literature. The difference observed between the coefficients of Z–R relations for various types of rains are essentially due to the differences in small-drop concentration.

APPENDIX

The Measurement of Small Drops with the JWD

According to Joss and Waldvogel (1993, personal communication) there are two different sources (S) of error affecting the measurement of small drops with the JWD: (S_1) acoustic noise from the surrounding and (S_2) ringing of the sampling area (a styrofoam cone) when it is hit by the drops.

If no care is taken in the setting up of the JWD, the effect of S_1 can be dramatic. In the JWD, an electronic circuitry is incorporated that continuously sets a noise threshold preventing any noise from being counted as drops. True drops producing signals below this threshold are lost. The noises provoking the rising of the threshold are, for example, thunder, motors, and electrical rotating machines (notably an electrical generating set used to supply the measuring devices in presence of thunderstorms during field observation campaigns) but also the rain itself from its impact on noisy surfaces such as water surface and especially metal sheets covering most of the roofs in the tropical areas. Metal sheets generate a noise strongly dependent on rain rate. Acoustic noise perturbation on JWD measurements can be reduced to a minimum and can almost be eliminated by proper setup of the transducer. This was done when collecting the data used in this present work. Usually, the JWD transducer was set up on a massive wood piece in the middle of a grassy area or on a carpet, away from buildings and noise sources.

Tests on the reduction of the acoustic noise effect in JWD are simple to perform by measuring the threshold voltage and by varying the intensity or distance of artificial noise sources.

The second source or effect (S_2) cannot be reduced by any preventive caution, but it can be corrected by mathematical methods. For this purpose Joss and Waldvogel (1993, personal communication) using theoretical and practical information about the dead time of the instrument after a drop pulse and information about the frequency and the size of the drops, developed the following formula:

$$N_i^* = N_i \exp\left[\frac{0.035}{T} \sum_{D_k=0.85D_i}^{D_{20}=5.25\text{ mm}} N_k \times \log \frac{D_k}{(0.85D_i - 0.25)}\right], \quad \text{(A1)}$$

where N_i is the number of drops in channel i without correction, N_i^* is the number of drops in channel i with correction, and T is the sampling time in seconds.

A drop of the i channel produces a dead time for all the k channels if

$$D_k < 0.85D_i.$$

In A1 the number of channels is 20 (case of the "standard" JWD delivered by the manufacturer). Of course A1 has to be modified if the channel distribution is different.

An example of corrected number of drops per channel is given in Table A1. The spectral parameters corresponding to the examples of Table A1 can be found in Table A2.

The JWD ability to detect small drops and the efficiency of the Joss–Waldvogel formula can be quali-

TABLE A1. Four examples of DSD correction using the Joss–Waldvogel formula A_1. Here U and C stand for uncorrected drop number and corrected drop number, respectively.

DSD number		Channel number																			
		1	2	3	4	5	6	7	8	9	10	11	12	13	14	15	16	17	18	19	20
1	U	14	16	33	42	29	41	50	30	20	27	53	25	19	8	7	1	3	1		
	C	49	40	67	73	46	57	63	35	22	29	56	26	19	8	7	1	3	1		
2	U	0	0	0	1	2	7	6	21	12	16	34	35	34	18	12	19	13	2	2	
	C	0	0	0	1	3	10	8	26	14	18	38	38	36	18	12	19	13	2	2	
3	U	1	8	6	18	32	40	51	36	39	30	53	33	45	21	28	24	12	7	2	3
	C	5	28	17	43	68	73	80	51	51	37	62	37	48	22	29	24	12	7	2	3
4	U	0	0	0	8	6	28	64	60	34	29	95	79	48	28	31	33	18	8	8	2
	C	0	0	0	25	16	64	122	99	50	39	120	93	53	30	32	34	18	8	8	2

TABLE A2. Spectral parameters of the four DSDs of Table A1 calculated using the Joss–Waldvogel formula A_1. Here U and C stand for uncorrected and corrected values respectively; W is the water content in g m^{-3}; R is the rain rate in mm h^{-1}; and Z is the radar reflectivity factor in mm^6 m^{-3}. Also, N_0 and λ are the exponential distribution parameters (1) in mm^{-1} m^{-3} and mm^{-1}, respectively.

DSD number		W (g m^{-3})	R (mm h^{-1})	Z (mm^6 m^{-3})	N_0 (mm^{-1} m^{-3})	λ (mm^{-1})
1	U	1.092	26.286	35 535.4	4698	1.92
	C	1.189	27.734	36 013.9	5626	1.96
2	U	1.848	52.126	121 423.3	3114	1.52
	C	1.920	53.758	122 637.2	3357	1.53
3	U	2.846	79.193	213 970.1	4004	1.45
	C	3.109	84.382	217 550.7	4813	1.49
4	U	3.947	110.433	297 534.2	5534	1.45
	C	4.441	121.109	306 015.0	7021	1.49

tatively tested using two ordinary spray nozzles, one producing the small-drop component (SDC) of the DSD and the other the large-drop component (LDC) of the DSD. Using a JWD transducer *having the original sensitivity,* SDC and LDC can be observed separately and together for different values of R. Figure A1 is an example of results. It suggests the *qualitative* conclusion that in the presence of a heavy rainfall a significant SDC can be observed using the JWD. Of course, in the case of a heavy rainfall with DSD having very low SDC, there is a level at which part of the SDC can remain undetected by the JWD. For the rain rate concerned by the present work (see Table 2 showing that up to R_7, rain rate is smaller than 60 mm h^{-1}) this shortcoming of JWD is only of minor consequence and cannot explain the rarity of small drops in tropical rainfall. Moreover Fig. 8 clearly shows that tropical DSDs are poor in small drops even for low rain rate.

As arguments complementary to the preceding, integrated quantities can be considered. Figure A2 shows for the eight distributions of sample E_3 (cf. Fig. 2 and Table 2) the comparison of the rainfall rate corresponding to each distribution (i.e., that the JWD measures),

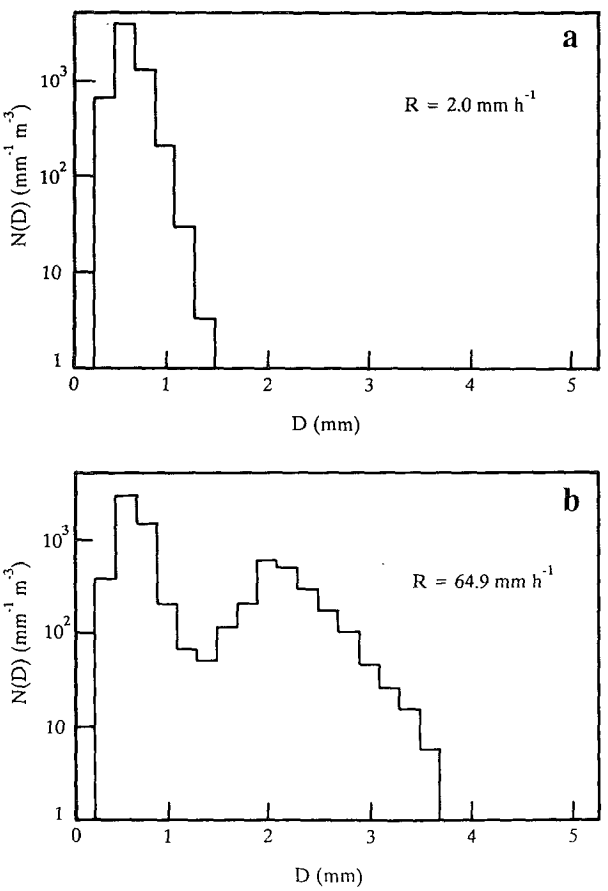

FIG. A1. Spray nozzle–generated DSDs observed using JWD. (a) Small-drop component; (b) small-drop and large-drop components. Here R is rain rate.

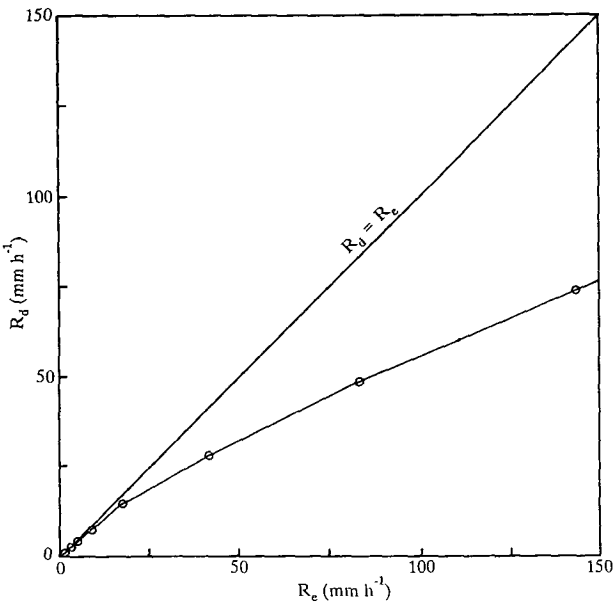

FIG. A2. Comparison of rain rates R_d measured with the JWD for the eight distributions of the E_3 sample with the exponential corresponding value R_e. The diagonal represents $R_d = R_e$.

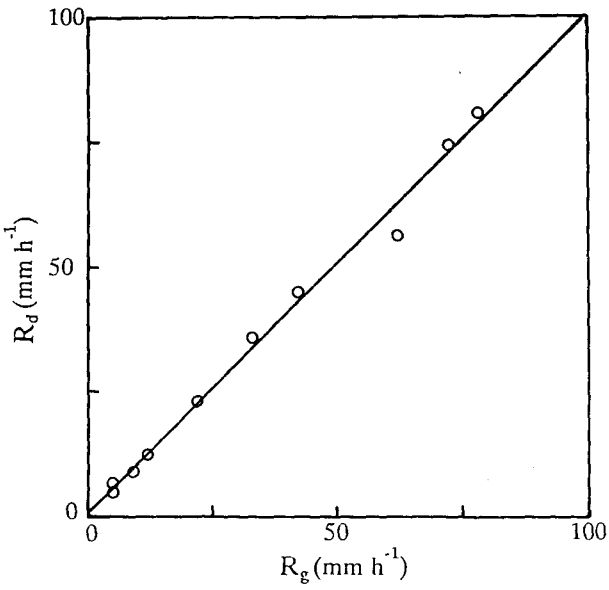

FIG. A3. Comparison of rain rates R_d measured with the JWD and R_g measured with a tipping bucket rain gauge on 17 August 1988 on a squall line in Niamey (Niger). The straight line is the regression curve [Eq. (A5)].

that is, R_d, with the R_e rain rate obtained with the same distributions for the drop size larger than the mode and the hypothesis that the classes of sizes below the mode are in conformity with the exponential distribution (1). By definition, we have

$$R = a\frac{\pi}{6}\int_0^\infty D^3 N(D)V(D)dD, \qquad \text{(A2)}$$

where a is a coefficient depending in the units and $V(D)$ the terminal fall velocity in still air given by (20). Replacing $N(D)$ with (1), we obtain, with R in mm h^{-1} (i.e., $a = 3.6 \times 10^{-3}$), N_0 in mm^{-1} m^{-3}, and λ in mm^{-1},

$$R_e = 0.105 N_0 \lambda^{-4.67}. \qquad \text{(A3)}$$

The values of N_0 and λ used in this equation to obtain R_e are those of Table 2, that is, those obtained by fitting to the values of $N(D)$ for $D > D_c$. We observe in Fig. A2 that R_e becomes much greater than R_d as rainfall rate increases. The difference is significant for $R > 20$ mm h^{-1} (+36% for $R = 30$ mm h^{-1}, +100% for $R = 150$ mm h^{-1}). Thus, if the decrease of the proportion of small drops when R increases is an artifact, the comparison of the rates determined by the disdrometer and by a reference instrument must show a significant difference, increasing with R.

Figure A3 shows the comparison of the rain rates determined by the JWD after correction for the acoustic noises (R_d) and by a tipping bucket rain gauge (R_g) placed near the JWD during the passage of a squall line on 7 August 1988 at Niamey (Niger). The rain gauge gives a measurement every 5 min. The data of the JWD were thus added up on 5-min periods and converted into average rain rates. The regression of the experimental points gives

$$R_d = 0.995 R_g + 0.916, \qquad \text{(A4)}$$

with $\rho = 0.996$. The JWD and the rain gauge thus measure the same rain rates.

Figure A4 (after Lefeivre 1993) shows the comparison of the total rain measured at Boyelé (Congo) between June 1988 and June 1989 (sample E3) with the JWD (corrected for the acoustic noises) (H_d), and with a simple adding rain gauge (H_e) placed near the disdrometer. Sixty-two events were considered, mostly squall lines. Each event is represented by one point in Fig. A4. The results show that 52% of the JWD measurements correspond to rates above 15 mm h^{-1} with $R_{max} = 170$ mm h^{-1}.

The regression has the following expression:

$$H_d = 1.087 H_e - 0.163, \qquad \text{(A5)}$$

with $\rho = 0.978$.

The disdrometer used at Boyelé has a systematic bias of about +8% compared with the pluviometer but no significant bias varying with R.

From the various arguments presented above, it can be concluded that the JWD, protected from acoustic noise and corrected for the S_2 effect, correctly measures

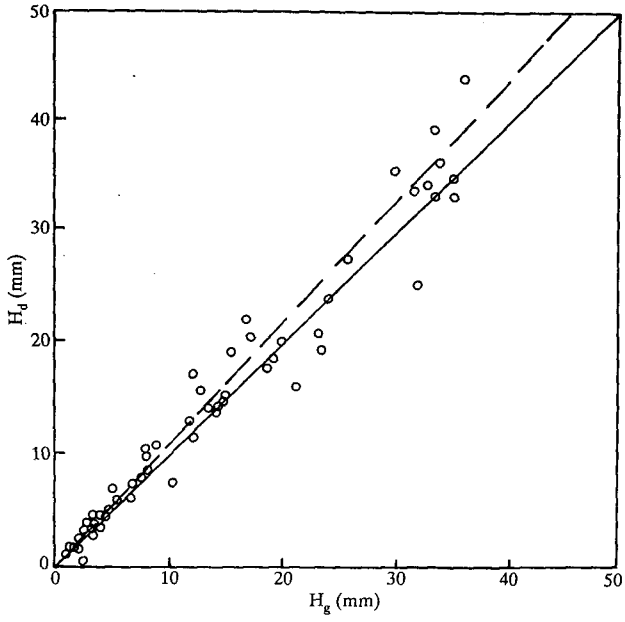

FIG. A4. Comparison of the cumulated rain heights H_d measured with the JWD with the cumulated rain heights H_g measured with a rain gauge for 62 rainy events observed from June 1988 to June 1989 in Boyelé (Congo). The solid line (diagonal) corresponds to $H_e = H_g$. The dashed line is the regression line [Eq. (A6)] (from Lefeivre 1993).

the rainfall rates and that the lack of small drops compared with the exponential that can be indicated by this instrument are, for the most part, real and not instrumental.

Acknowledgments. The authors would like to thank all the contributors to the disdrometer database, notably the University of Abidjan in Ivory Coast, the ORSTOM mission in Niger, and the University of Brazzaville in Congo. The authors also are very grateful for the personal communication they received from Drs. J. Joss and A. Waldvogel about the correction of the disdrometer data and for the permission to publish their formula in this present paper. Thanks are also due to Dr. R. List and to anonymous reviewers for helpful comments and criticisms.

REFERENCES

Asselin de Beauville, C., R. H. Petit, G. Marion, and J. P. Lacaux, 1988: Evolution of peaks in the spectral distribution of raindrops from warm isolated maritime clouds. *J. Atmos. Sci.*, **45**, 3320–3332.

Atlas, D., and C. W. Ulbrich, 1977: Path and area-integrated rainfall measurement by microwave attenuation in the 1–3 cm band. *J. Appl. Meteor.*, **16**, 1322–1331.

Blanchard, D. C., and A. T. Spencer, 1970: Experiments on the generation of raindrop-size distributions by drop breakup. *J. Atmos. Sci.*, **27**, 101–108.

Brazier-Smith, P. R., S. G. Jennings, and J. Lathan, 1973: Raindrop interaction and rainfall rates within clouds. *Quart. J. Roy. Meteor. Soc.*, **99**, 260–272.

Brown, P. S., 1991: Parameterization of the evolving drop-size distribution based on analytic solution of the linearized coalescence breakup equation. *J. Atmos. Sci.*, **48**, 200–210.

——, and S. N. Whittlesey, 1992: Multiple equilibrium solutions in Bleck-type models of drop coalescence and breakup. *J. Atmos. Sci.*, **49**, 2319–2324.

Cataneo, R., and G. E. Stout, 1968: Raindrop-size distribution in humid continental climates, and associated rainfall rate–radar reflectivity relationships. *J. Appl. Meteor.*, **7**, 901–907.

Chandrasekar, V., and V. N. Bringi, 1987: Simulation of radar reflectivity and surface measurements of rainfall. *J. Atmos. Oceanic Technol.*, **4**, 464–478.

Desbois, M., T. Kayiranga, B. Gnamien, S. Guessous, and L. Picon, 12988: Characterization of some elements of the Sahelian climate and their interannual variations. *J. Climate*, **1**, 868–904.

Feingold, G., and Z. Levin, 1986: The lognormal fit to raindrop spectra from frontal convective clouds in Israel. *J. Climate Appl. Meteor.*, **25**, 1346–1363.

——, S. Tzivion, and Z. Levin, 1988: Evolution of raindrop spectra. Part I: Solution to the stochastic collection/breakup equation using the method of moments. *J. Atmos. Sci.*, **45**, 3387–3399.

Fujiwara, M., 1965: Raindrop size distributions from individual storms. *J. Atmos. Sci.*, **22**, 585–591.

Hodson, M. C., 1986: Raindrop size distribution. *J. Climate Appl. Meteor.*, **25**, 1070–1074.

Jones, D. M. A., 1992: Raindrop spectra at the ground. *J. Appl. Meteor.*, **31**, 1219–1225.

Joss, J., and A. Waldvogel, 1967: Ein Spectrograph für Niederschlagstropfen mit automatisher Auswertung. *Pure Appl. Geophys.*, **68**, 240–246.

——, and E. G. Gori, 1976: The parameterization of raindrop size distributions. *Riv. Ital. Geofis.*, **3**, 273–283.

——, and ——, 1978: Shapes of raindrop size distributions. *J. Appl. Meteor.*, **17**, 1054–1061.

Lefeivre, B., 1993: Etude expérimentale et par modélisation des caractérisiques physiques et chimiques des précipitations collectées en forêt équatoriale africaine. Doctoral thesis, Université Paul Sabatier, 308 pp.

List, R., 1988: A linear radar reflectivity–rainrate relationship for steady tropical rain. *J. Atmos. Sci.*, **45**, 3564–3572.

——, and J. R. Gillespie, 1976: Evolution of raindrop spectra with collision induced breakup. *J. Atmos. Sci.*, **33**, 2007–2013.

——, N. R. Donaldson, and R. E. Stewart, 1987: Temporal evolution of drop spectra to collisional equilibrium in steady and pulsating rain. *J. Atmos. Sci.*, **44**, 362–372.

Low, T. B., and R. List, 1982: Collision, coalescence and breakup of raindrops. Part II: Parameterization of fragment size distributions. *J. Atmos. Sci.*, **39**, 1607–1618.

Marshall, J. S., and W. M. K. Palmer, 1948: The distribution of raindrops with size. *J. Meteor.*, **5**, 165–166.

McFarquhar, G. M., and R. List, 1991: The evolution of three-peak raindrop size distributions in one-dimensional shaft models. Part II: Multiple pulse rain. *J. Atmos. Sci.*, **48**, 1587–1595.

——, and ——, 1992: Observations of raindrop size-distributions and fluctuations in tropical rainfall as measured by a disdrometer and a Doppler radar. Preprints, *11th Int. Conf. on Clouds and Precipitation*, Montreal, Quebec, Canada, Amer. Meteor. Soc., 165–168.

Mueller, E. A., and A. L. Sims, 1966: Radar cross sections from drop size spectra. Tech. Rep. ECOM-00032F, Illinois State Water Survey, 110 pp.

Pasqualucci, F., 1982: The variation of drop size distribution in convective storms: A comparison between theory and measurement. *Geophys. Res. Lett.*, **9**, 839–841.

Sauvageot, H., and G. Despaux, 1989: SANAGA—Un système d'acquisition numérique et de visualisation des données radar pour la validation des estimations satellitaires de précipitations. *Veille Climatique Satellitaire*, **30**, 51–55.

Sekhon, R. S., and R. C. Srivastava, 1971: Doppler observations of drop size distributions in a thunderstorm. *J. Atmos. Sci.*, **28**, 983–994.

Sheppard, B. E., 1990: Effect of irregularities in the diameter classification of raindrop by the Joss–Waldvogel disdrometer. *J. Atmos. Oceanic Technol.*, **7**, 180–183.

Smith, P. L., Z. Liu, and J. Joss, 1993: A study of sampling-variability effects in raindrop size observations. *J. Appl. Meteor.*, **32**, 1259–1269.

Srivastava, R. C., 1978: Parameterization of raindrop size distributions. *J. Atmos. Sci.*, **35**, 108–117.

——, 1982: A simple model of particle coalescence and breakup. *J. Atmos. Sci.*, **39**, 1317–1322.

Steiner, M., and A. Waldvogel, 1987: Peaks in raindrop size distributions. *J. Atmos. Sci.*, **44**, 3127–3133.

Ulbrich, C. W., 1983: Natural variations in the analytical form of the raindrop size distribution. *J. Climate Appl. Meteor.*, **22**, 1764–1775.

Valdez, M. P., and K. C. Young, 1985: Number fluxes in equilibrium raindrop populations: A Markov chain analysis. *J. Atmos. Sci.*, **42**, 1024–1036.

Willis, P. T., and P. Tattelman, 1989: Drop-size distribution associated with intense rainfall. *J. Appl. Meteor.*, **28**, 3–15.

Zawadski, I., and M. de Agostinho Antonio, 1988: Equilibrium raindrop size distributions in tropical rain. *J. Atmos. Sci.*, **45**, 3452–3459.